Results in Physics 6 (2016) 1051–1058

Contents lists available at ScienceDirect

Results in Physics

journal homepage: www.journals.elsevier.com/results-in-physics

Yttrium doped TiO_2 porous film photoanode for dye-sensitized solar cells with enhanced photovoltaic performance

Xiaofei Qu, Yuchen Hou, Meihua Liu, Liang Shi, Mingqian Zhang, Hongbing Song, Fanglin Du *

College of Materials Science and Engineering, Qingdao University of Science & Technology, Zhengzhou Road 53, Qingdao 266042, China

ARTICLE INFO

Article history:
Received 12 November 2016
Accepted 14 November 2016
Available online 16 November 2016

Keywords:
Dye sensitized solar cells
TiO_2 photoanode
Rare earth doping
Yttrium

ABSTRACT

In this paper, TiO_2 photoanodes were doped with yttrium under different doping concentrations via hydrothermal method and further employed to assemble dye-sensitized solar cells (DSSCs). XRD, XPS, SEM, TEM, UV–Vis DRS and PL measurements were carried out to investigate the yttrium doping effects on crystal structure, chemical status, optical properties and dye loading capacity of the photoanodes. The photovoltaic performance of the photoanodes with various yttrium doping concentration was measured by recording the photocurrent-photovoltaic curves, and the result indicated that TiO_2:0.006 Y exhibited the best power conversion efficiency with high short circuit current density (J_{sc}) and open circuit voltage (V_{oc}). This improvement may be due to the enhanced visible light harvesting, increased dye loading capacity and reduced photoelectron recombination.

Introduction

The solar to electric power has been considered to be a promising solution to resolve the energy crisis [1]. Although traditional silicon based solar cell owns many advantages such as high energy conversion efficiency and stability [2], its application is restricted due to the high cost. So some substitutes for silicon based solar cells have been investigated. For example, Cu_2O solar cell is attractive owing to high mobility for majority carriers, abundant raw materials and low cost [3,4]. Cu_2ZnSnS_2 (CZTS) thin film solar cell also receives increased research interest because of high sunlight absorption coefficient and tunable bandgap [5,6]. Since the prototype firstly reported by O'Regan and Gratzel's in 1991 [7], dye-sensitized solar cells (DSSCs) have attracted more and more attentions [8–11]. Typically, a DSSC consists of a porous photoanode sensitized by dye molecular to absorb incident sunlight, an electrolyte containing I^-/I_3^- redox couple and a platinum-coated counter-electrode [12–14].

In the application of DSSCs, TiO_2 is attractive because of its stability and moderate charge transport capability. Strategy widely used to improve the efficiency of the cells was to suppress the charge recombination by passivating the recombination centers at the TiO_2 porous film with the addition of 4-*tert*-butylpridine (TBP) to the electrolyte [15]. Moreover, the cell's performance could also be improved by surface modification with the formation of barrier layer, which could reduce the dark current caused by the interfacial charge recombination. For example, modification of TiO_2 layer with gadolinium-containing layer as an energy barrier to inhibit back transfer of electron [16] led to an enhanced photovoltaic performance for DSSC. In addition, the modification layer may enhance the adsorption of carboxyl groups in N719 dye molecule, leading to increased dye loading capacity and enhanced cell performance [17].

Because rare earth elements often own 4f orbits and vacant 5d orbits, they have various intermediate energy states which permits multiple electron configuration, which provides them great potential in various functional materials, such as photocatalysts [18], laser host materials [19] and phosphors [20]. In the field of DSSCs, strategy of rare earth doping is also used by many people to achieve enhanced performance. Zhang et al. doped TiO_2 photoanode with cerium ions. Due to the improved electrons injection from the dye to the TiO_2 photoanode and enhanced separation of the photoelectron-hole pairs derived from Ce^{4+}/Ce^{3+} oxidized states in the TiO_2 films, the cell performance was improved [21]. Liu et al. modified TiO_2 nanotubes with Sm_2O_3 and the results showed that Sm_2O_3 acted not only as a down-conversion luminescence material to increase sunlight harvest, but also as an surface energy barrier to reduce electron recombination [22]. Shogh et al. reported that due to enhancement of electron injection efficiency, reduced trap states density, and electron transport time [23], after doping TiO_2 nanoparticles in the photoanode with neodymium, the cell's efficiency was increased.

* Corresponding author.
E-mail address: dufanglin2008@hotmail.com (F. Du).

http://dx.doi.org/10.1016/j.rinp.2016.11.021
2211-3797/

The yttrium doped TiO_2 photoanodes were also studied [24–26] and the relating works were all applied as follows: the yttrium source materials (YCl_3, $Y(NO_3)_3{\cdot}6H_2O$ or the Y_2O_3:Eu^{3+} powder) were dispersed in the TiO_2 colloid (TBOT,TTIP:TEOA or TiO_2) to form the mixture first, and then experienced aging or sintering process, and finally yttrium doped TiO_2 was obtained. At last, the obtained doped TiO_2 was transferred onto the surface of fluroine doped tin oxide (FTO) conductive sheet glass. In these works, yttrium species could be distributed in the TiO_2 film photoanodes randomly.

In this work, a different process was applied: First, the obtained TiO_2 paste was spread on the fluroine doped tin oxide (FTO) conductive sheet glass. After sintered, the prepared TiO_2 photoanodes were placed in $Y(NO_3)_3$ solution. After taken out and further annealed, the obtained yttrium-doped TiO_2 photoanode was obtained. The nitrate solution used in our work is easier to penetrate into the porous film, so Y_2O_3 could cover on TiO_2 film surfaces during the second annealing process. Compared with other work where yttrium species were randomly distributed, in our paper, Y_2O_3 will mainly cover on TiO_2 surfaces, which could have obvious advantage: a coating shell was covered on the TiO_2 porous film. The shell for the modified samples as a powerful energy barrier made it hard for the injected electrons to recombine with dyes or oxidized redox couple (Ox) in the electrolytes.

Experimental section

Fabrication of photoanode

The TiO_2 pastes were prepared similar to Xu's work [27]. A typical process was described as follows: The starting materials were Tetra-n-butyl Titanate (TNB, $C_{16}H_{36}O_4Ti$, 97%, Energy Chemical Co., Ltd.) All chemicals were used as received without further purification. 10 mL of TNB was dropped into 100 mL of deionized water under vigorous magnetic agitation of about 1700 rpm at the room temperature. After 30 min, the mixture was pump-filtrated, and washed by deionized water and ethanol for several times to obtain clean dehydrated powders. Then, the powders were transferred into a flask and 0.8 mL of nitric acid, 10 mL of acetic acid were dropwise added into the flask. The mixture was then carefully magnetically stirred with the speed of 1000 rpm in a 80 °C waterbath for 15 min. After that, the volume of the mixture was adjusted to about 170 mL with deionized water. The obtained mixture was heated in a sealed environment in 80 °C waterbath and kept magnetically stirred at 1500 rpm for 10 min. About 145 mL of the obtained blue colloid was transferred into three Teflon-lined autoclaves whose volume was about 70 mL, and about 35 mL of the blue colloid was reserved for further use. The autoclaves were heated at 200 °C for about 12 h. After removing supernatant from the three autoclaves, about 45 mL "white colloid Ⅰ" was obtained. After that, about 0.28 g of P25, 20 mL blue colloid was added into the obtained white colloid and magnetically stirred at 1500 rpm under room temperature for 3 min. Before put into two Teflon-lined autoclaves, the mixture was further mixed with ultrasonic treatment. The autoclaves were heated again at 200 °C for about 12 h. 1 mL of OP-Emulsifier was added into 10 mL of ethanol to form a homogeneous solution A. After removal of supernatant, about 0.55 g PEG-20000 and 0.70 mL of solution A was added into the obtained "white colloidⅡ" to form a homogeneous mixture. The mixture was heated in a 80 °C waterbath and carefully kept magnetically stirred at the speed of 250 rpm for 1 h. Hereby, the TiO_2 paste was obtained.

The obtained TiO_2 pastes are spread on the fluorine doped tin oxide (FTO) conductive sheet glass with a doctor-blade method. The working area and thickness of the TiO_2 thin film was controlled using 3 M Scotch tapes. The area for TiO_2 photoanodes was approximately 0.25 cm^2 and the thickness was about 7 μm. After sintered at 450 °C for 30 min, the prepared TiO_2 photoanodes were placed in $Y(NO_3)_3$ solution (0.006 mol/L) contained by a Teflon-lined steel autoclave and kept at 100 °C for 12 h. The obtained photoanodes were then washed with deionized water and ethanol. After drying process, the photoanodes were annealed at 500 °C for 30 min. The obtained yttrium-doped TiO_2 photoanode was obtained and denoted as TiO_2:0.006 Y. Similarly, different photoanodes (TiO_2:0.015 Y, TiO_2:0.025 Y) were also fabricated. Undoped TiO_2 photoanode was also prepared as comparison.

Cell assembly

First, the obtained photoanodes were soaked into N719 dye solution (0.5 mM in ethanol) for 24 h. A platinum coated FTO glass was employed as the counter electrode. After drying, the

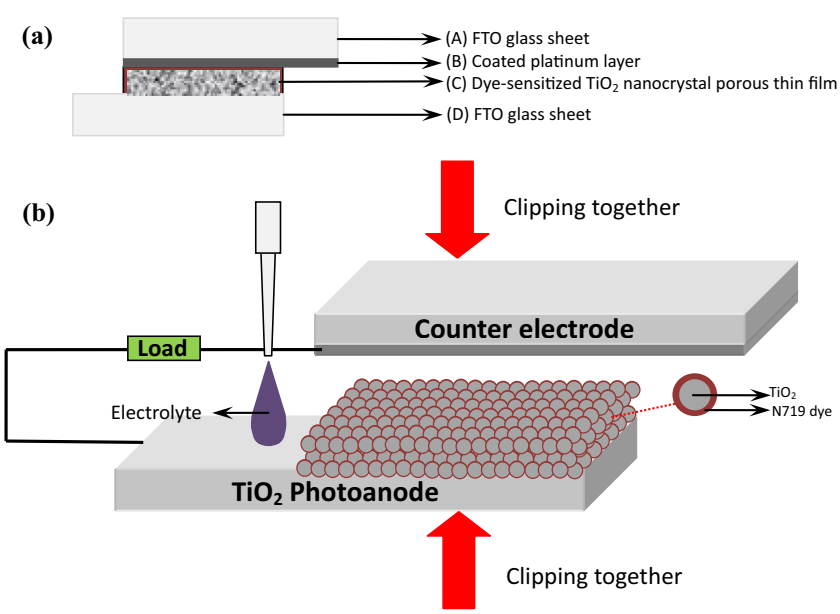

Fig. 1. Schematic illustration for the cell structure: (a) Overall schematic illustration (b) Detailed cell structure illustration.

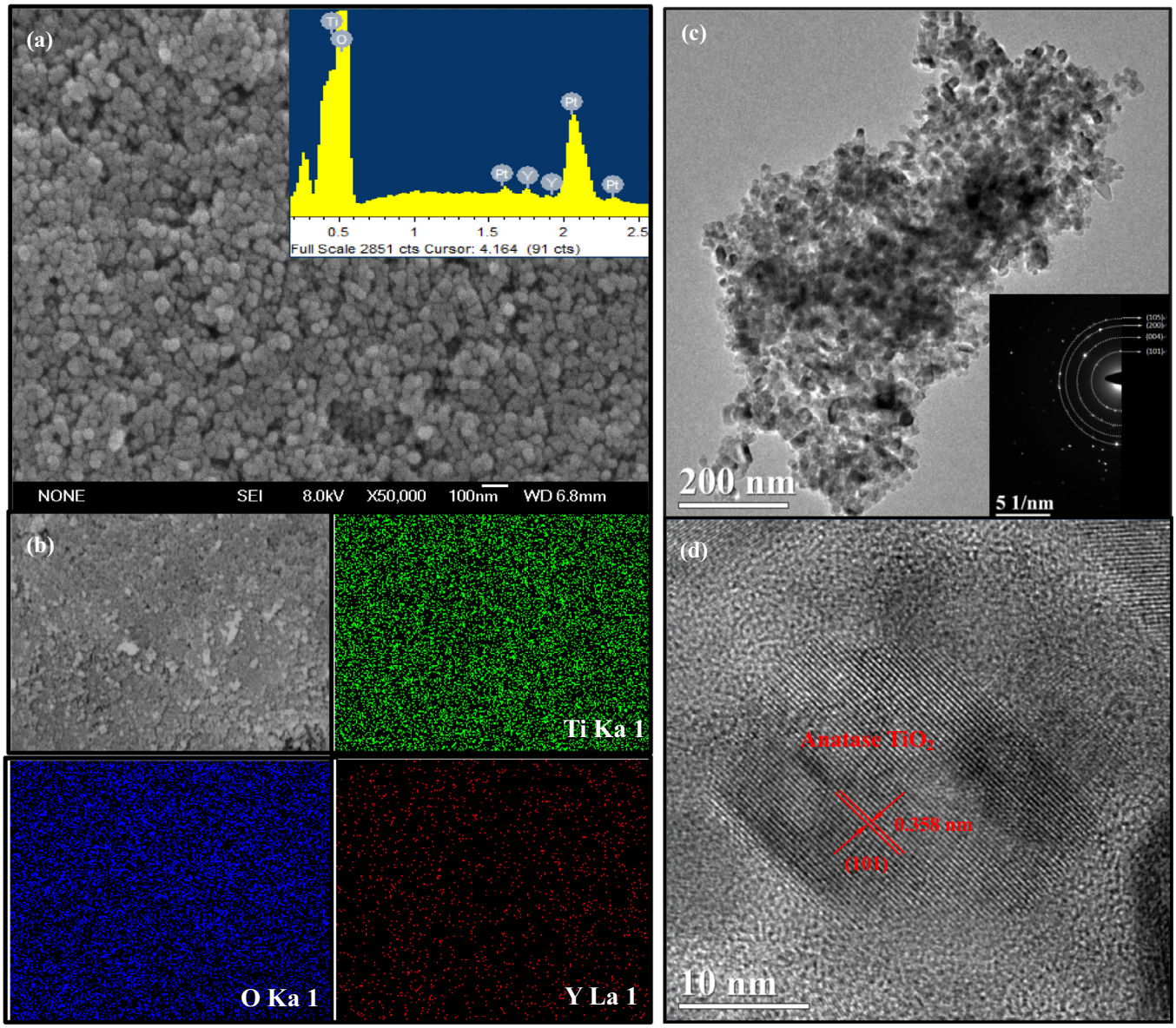

Fig. 2. (a)–(b): (a) SEM image (insert: EDS pattern) and (b) SEM Mapping of Ti, O, Y of the prepared TiO_2:0.015 Y photoanode; (c)–(d): (c) TEM image (insert: SAED pattern) and HR-TEM image of the TiO_2:0.015Y powder peeled from photoanode.

dye-sensitized photoanode and the platinum coated FTO were tightly clipped together. Then, A drop of electrolyte (0.1 M KI, 50 mM I_2, 0.5 M 4-*tert*-butylpyridine (TBP) and 0.6 M 1,2-dimethyl-3-propylimidazolium iodide (DMPII) in acetonitrile) was added into the space between the two electrodes. Hereby the cell for subsequent photovoltaic measurements was fabricated. Fig. 1 was a simple schematic illustration for the assembled cell structure.

Characterization

SEM and EDS element mapping were obtained by a field emission scanning electron microscope (FESEM, JEOL Ltd., Japan, JSM-6700F). TEM and SAED tests were performed on a field-emission transmission microscope (FETEM, JEOL Ltd., Japan, JEM-2100). XRD analysis was performed with a XRD instrument (Rigaku Corporation, Japan, D-MAX2500 diffractometer). XPS was performed on a X-ray photoelectron spectrometer (Kratos Corporation, UK, XSAM800). The UV–Vis spectra were obtained with a UV–Vis spectrometer (Varian Corporation, USA, Cary500). PL spectra were measured at the room temperature under the excitation wavelength of 276 nm with a Fluorescence spectrometer (Edinburgh Instrument, UK, FLS920). The photovoltaic performance of the DSSCs were evaluated by recording the photocurrent-photovoltaic curves using a electrochemical workstation (CHI660D, Chenhua Instrument Co., LTD, China) in a three-electrode configuration under one sun AM 1.5G illumination with an output power of 100 mW cm^{-2} produced by a solar light simulator (Oriel Sol 3A class AAA). A 450 W Xenon lamp (Newport 6991, Newport Corporation, USA) was employed as the light source.

Electrochemical impedance spectroscopy (EIS) measurements were conducted under an open circuit voltage in a frequency ranging from 10^{-2} Hz to 10^5 Hz and ac amplitude of 10 mV at room temperature.

The dye adsorption capacity of the samples was measured as follows: N719 dye-sensitized TiO_2 photoanodes with active area (0.25 cm^2) were immersed into 5.0 mL of 0.1 M NaOH solution. After the N719 dye molecules fully detached from the surface of

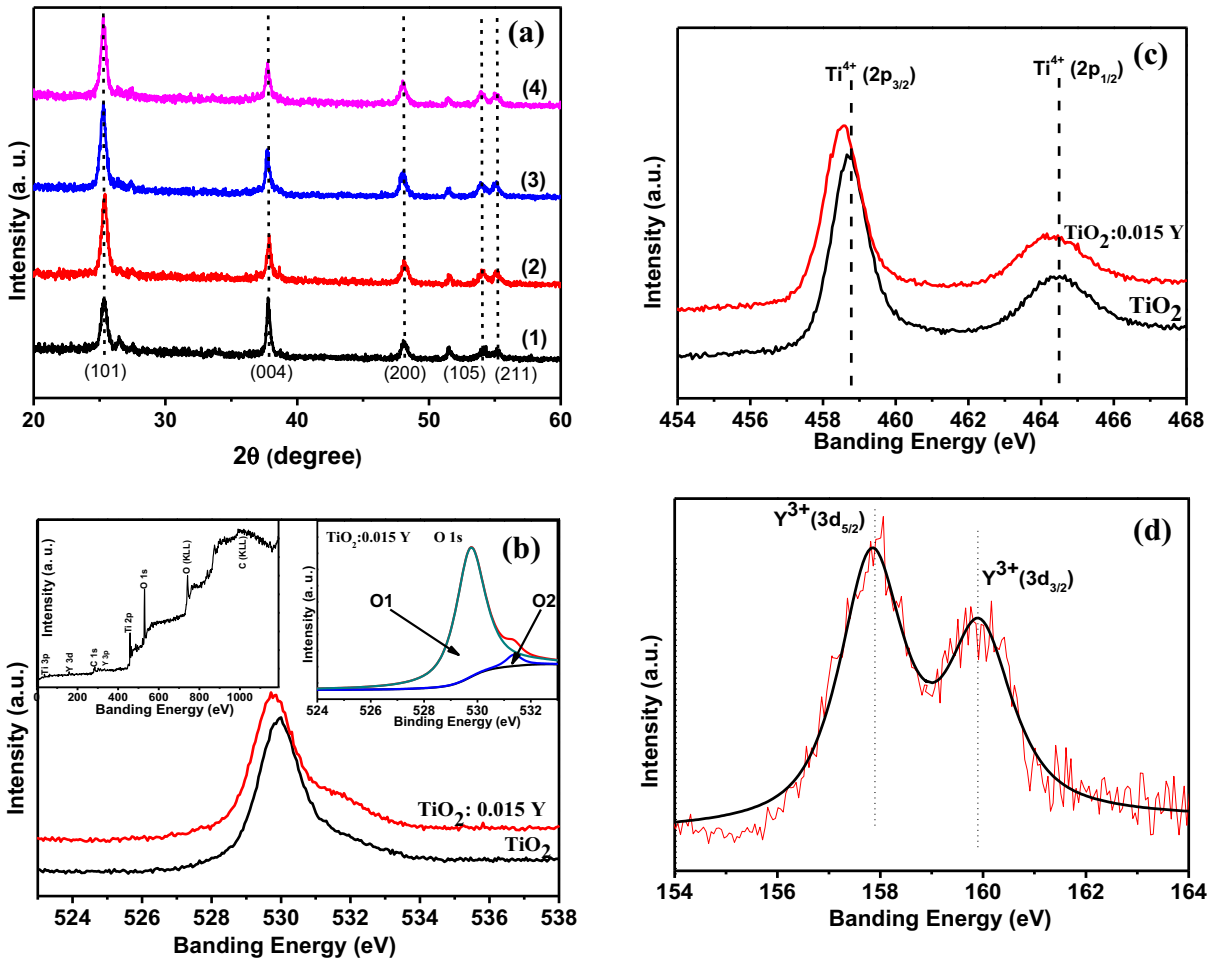

Fig. 3. (a) XRD patterns of different photoanodes: (1) TiO_2; (2) TiO_2:0.006 Y; (3) TiO_2:0.015 Y (4) TiO_2:0.025 Y (b)–(d): The XPS spectra of TiO_2 and TiO_2:0.015 Y: (b) O 1s (c) Ti 2p and (d) Y 3d. Insert of (b): Left side: XPS overall scanning spectrum; Right side: Fitted XPS results for O 1s of TiO_2:0.015 Y.

the TiO_2 photoanodes, the resulting solutions were characterized by UV–Vis spectroscopy.

Results and discussion

Morphology

Morphology of the prepared TiO_2:0.015 Y was characterized via SEM and TEM (Fig. 2). From Fig. 2a, the porous nature for photoanode TiO_2:0.015 Y could be seen. In the EDS pattern (insert of Fig. 2a), in addition to the Ti and O element from TiO_2, existence of Y element could also be observed. The SEM-EDS mapping of TiO_2:0.015 Y in Fig. 2b indicated that the Y element was dispersed uniformly in the photoanode. From Fig. 2c, it could be seen that the spherical nanoparticles exhibited a size of ~25 nm. The SAED (insert of Fig. 2c) confirmed the anatase crystallite nature for the prepared sample. Form the lattice fringes of the nanocrystal (Fig. 2d), the space of the (1 0 1) plane for the TiO_2:0.015 Y sample was about 0.358 nm, further indicating the nature of anatase TiO_2.

Crystal structure and chemical status analysis

Crystal structure of the samples was further investigated through XRD tests. From Fig. 3a, no obvious difference was observed between the peak characteristics of the doped and undoped TiO_2 photoanodes. The XRD peaks located at $2\theta = 25.4°$, 37.7°, 48.1°, 54.0° and 55.1°in the spectra of both undoped and doped thin films are easily identified as (1 0 1), (0 0 4), (2 0 0), (1 0 5) and (2 1 1) crystallographic planes of a crystallinity anatase form (JCPDS 21-1272).

As we know, the distribution status of the present rare earth ions could also be reduced to three kinds of spatial location: lattice (replacing Ti^{4+} and interstitial void), grain boundary and particle surface. Because the ion radius of Y^{3+} (0.90 Å) is much larger than that of Ti^{4+} (0.61 Å), it was hard for it to enter the TiO_2 lattice.

But in our experiment, the used yttrium nitrate solution was easier to penetrate into the porous film, so Y_2O_3 can cover on TiO_2 surfaces or form the sub-grains among the grain boundaries during the second annealing process. For Y doped photoanodes, no additional characteristic peaks (such as Y_2O_3) except anatase TiO_2 was found, which may be attributed to the low content and high dispersity of yttrium species.

From XPS overall scanning result (insert of Fig. 3b, left), in addition to the Ti and O elements, existence of Y in the doped samples could be confirmed. From Fig. 3b, it was shown that the peak position of bare TiO_2 sample matched well to the binding energy of O—Ti—O bonds with well symmetrical peak shape, indicating signal existing state of O element [28]. But, the asymmetric shape of the peak for TiO_2:0.015 Y (denoted as TiO_2/Y_2O_3) indicated different existing status of O. After peak fitting, two peaks located at 529.75 eV and 531.29 eV was separated (insert of Fig. 3b, right). The peak located at about 529.75 eV (O_1) may be assigned to O element bounded to Ti in the TiO_2 lattice. For the peak located at

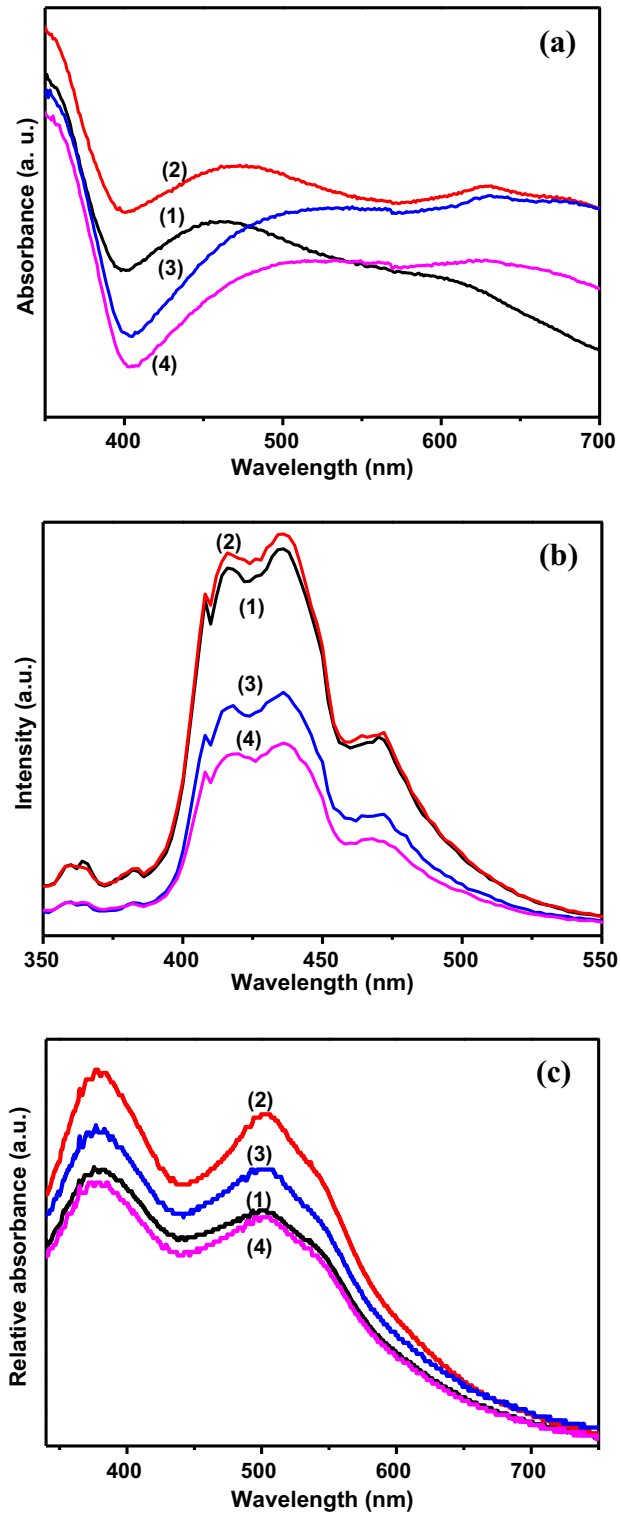

Fig. 4. (a) The UV–Vis DRS spectra; (b) The emission spectra (excited by 276 nm) and (c) result of dye loading capacity measurement of different TiO_2 photoanodes: (1) TiO_2; (2) TiO_2:0.006 Y; (3) TiO_2:0.015 Y; and (4) TiO_2:0.025 Y.

531.29 eV (O_2), it may be indexed to the presence of hydroxyl oxygen [29], which is beneficial for increased dye loading capacity and enhanced cell performance [17]. From the high-resolution XPS pattern of Ti 2p in Fig. 3c, for pure TiO_2, two peaks located at 458.8 eV and 464.5 eV were indexed to $Ti^{4+}_{(2p\ 3/2)}$ and $Ti^{4+}_{(2p\ 1/2)}$, respectively [21], indicating the Ti^{4+} valence state of Ti. However, for Y doping TiO_2 (TiO_2/Y_2O_3), the peak of Ti 2p exhibited a small shift

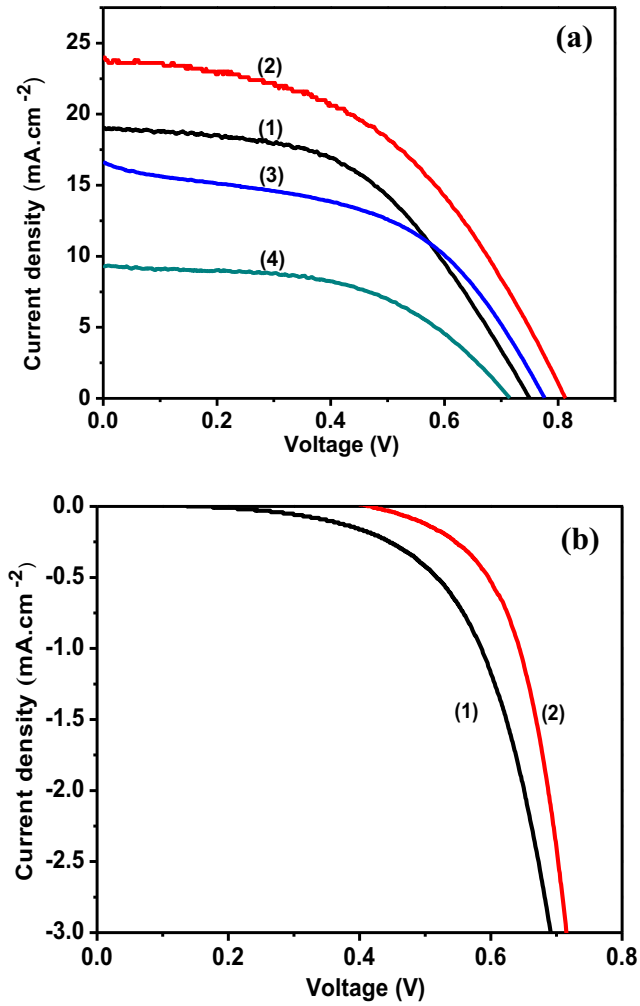

Fig. 5. The current-voltage (J-V) characteristic curve of the cells assembled with different photoanodes: (1) TiO_2; (2) TiO_2:0.006 Y; (3) TiO_2:0.015 Y; and (4) TiO_2:0.025 Y measured (a) under illumination of one sun (AM 1.5 G, 100 mW cm^{-2}) and (b) in the dark.

(~0.1 eV) towards lower banding energy, which may be attributed to formation of Y-O-Ti bond on the surface of TiO_2. In Fig. 3d, two peaks located at 157.84 eV and 159.87 eV was assigned to $Y^{3+}_{(3d\ 5/2)}$ and $Y^{3+}_{(3d\ 3/2)}$, respectively [30].

Light absorption properties

Fig. 4a exhibited the absorption characteristics of different samples prepared with the UV–Vis diffuse reflection spectra. It could be seen that in the visible light region (400–700 nm), all the doped samples showed an enhanced absorbance, leading to enhanced visible light photoresponse. With the increase of Y doping concentration, the absorption edge exhibited an apparent red-shift for TiO_2:0.006 Y, and then blue-shift for TiO_2:0.015 Y and TiO_2:0.025 Y. There are various explanations for the change of the optical absorption edge. Generally, the yttrium doping would lead to a red-shift of absorption edge [31,32]. In work of Niu et al. [31], red-shift of absorption edge was attributed to the charge transfer process between f electrons from Y^{3+} and conduction or valence band(CB or VB) of TiO_2, which lead to a lower optical band gap energy. While according to research work of Zhang et al. and Kumar et al. [33,34], blue-shift of absorption edge after yttrium doping was due to occupied states of Ti 3*d* and the up-shift of fermi level. In our concern, yttrium doping created dopant levels near the

Table 1
Photovoltaic characteristic parameters of DSSCs with different Y doping concentration.

Samples	V_{oc} (V)	J_{sc} (mA.cm^{-2})	FF (%)	η (%)
Pristine TiO_2	0.75	19.1	50.52	7.18
TiO_2:0.006Y	0.81	23.9	47.24	9.18
TiO_2:0.015Y	0.78	16.7	49.23	6.38
TiO_2:0.025Y	0,72	9.34	52.56	3.51

CB, resulting in red-shift of absorption edge and lower band gap. With the increase of doping concentration, enhanced dopant incorporation may cause gradual movement of CB, leading to absorption edge blue-shift and larger band gap.

The room temperature photoluminescence (PL) emission spectra of the samples (recorded at λ = 276 nm) were shown in the Fig. 4b, which could reveal the recombination rate of photogenerated charge carrier in the semiconductor. In our work, the PL spectra showed that the peak positions for all the doped and un-doped samples were similar, indicating that the yttrium doping didn't cause new luminescent phenomenon. For both the doped and undoped samples, the broadened peak at around 410 nm could be attributed to band gap recombination of host TiO_2, while the peak at 465 nm may be related with bound excitation luminescence derivated from the surface defect of TiO_2 [35]. With the increase of doping concentration, the intensity of the emission peak slightly increased for TiO_2:0.006 Y compared with the undoped TiO_2, and then continuously decrease of peak intensity could be observed for TiO_2:0.015 Y and TiO_2:0.025 Y. Decreased emission peak intensity could reflect suppressed recombination of the photo-generated carriers and longer carrier lifetime. The reason may be that with increased doping concentration, more traps were introduced into TiO_2 and more photoelectrons were trapped and kept from recombination, leading to an impaired photoluminescence emission intensity.

Dye loading capacity analysis

From Fig. 4c, it could be seen that with the increase of doping concentration, the characteristic absorption peak located at 520 nm increased, reaching to maximum for TiO_2:0.006Y and then decreased. In our concern, the increased dye loading capacity may be due to formation of Ti—O—Y complex between TiO_2 and yttrium species, which may generate lattice charge imbalance. To make up for this charge imbalance, more —OH radicals were absorbed, which increased the hydrophilicity. More —OH radical could combine more —COOH radical from the dye molecular and therefore improve the dye loading capacity. However, with the further increase of doping concentration, over-doping of yttrium in TiO_2 would result in the decrease in the electrode's porosity. And the decrease in the electrode's porosity may be responsible for the decreasing dye loading capacity.

Photovoltaic performance

Fig. 5a showed the J-V curves of the DSSCs with different TiO_2 photoanodes measured under illumination of one sun (AM 1.5G, 100 mW cm^{-2}). The corresponding values of photovoltaic characteristics were summarized in Table 1. For the DSSC using pure TiO_2 photoanodes, it exhibited a short circuit current density (J_{sc}) of 19.1 mA.cm^{-2}, an open circuit voltage (V_{oc}) of 0.75 V and fill factor (FF) of 50.52 %, yielding an overall power conversion efficiency (η) of about 7.18 %. For TiO_2:0.006 Y, the yttrium doping led to an increased J_{sc} (23.7 mA.cm^{-2}) and V_{oc} (0.81 V) with a power conversion efficiency of 9.18 %, which showed an improvement of 27.9 % compared with that for pure TiO_2. However, with increased doping concentration, J_{sc} and V_{oc} then decreased for TiO_2:0.015Y and TiO_2:0.025Y, leading to impaired efficiency of 6.38 % and 3.51 %. The increase in J_{sc} for TiO_2:0.006Y may be ascribed to its increased dye loading capacity and enhanced visible light harvesting ability which enhanced the photoelectron injection. In addition, reduced photoelectrons recombination and prolonged electron lifetime may also be the reason for the enhanced V_{oc}. However, with further increased of yttrium doping concentration, J_{sc} and V_{oc} dropped, and the power conversion efficiency decreased. However, with further increased of yttrium doping concentration, J_{sc} and V_{oc} dropped, and the power conversion efficiency decreased. The reason may be that: (1) Under excessive doping concentration, more traps and defects may be introduced into the TiO_2 lattice, which may severely trapped photogenerated electrons and inhibited electron transfer process, leading to impaired photocurrent [22–23,25]. (2) Excessive modification results in more Y_2O_3 immingled among the TiO_2 network, and then it's more difficult for electrons to transport due to the insulatibity [17,36].

As known, the dark current referred to backward transfer of electrons to recombine with oxidized species (I_3^- ions) in the electrolyte, which could greatly compromise the cell's performance [37]. From the J-V curves of the samples measured in the dark (Fig. 5b), the sample TiO_2:0.006Y owned a lower dark current density than TiO_2, which indicated it owned a slower recombination

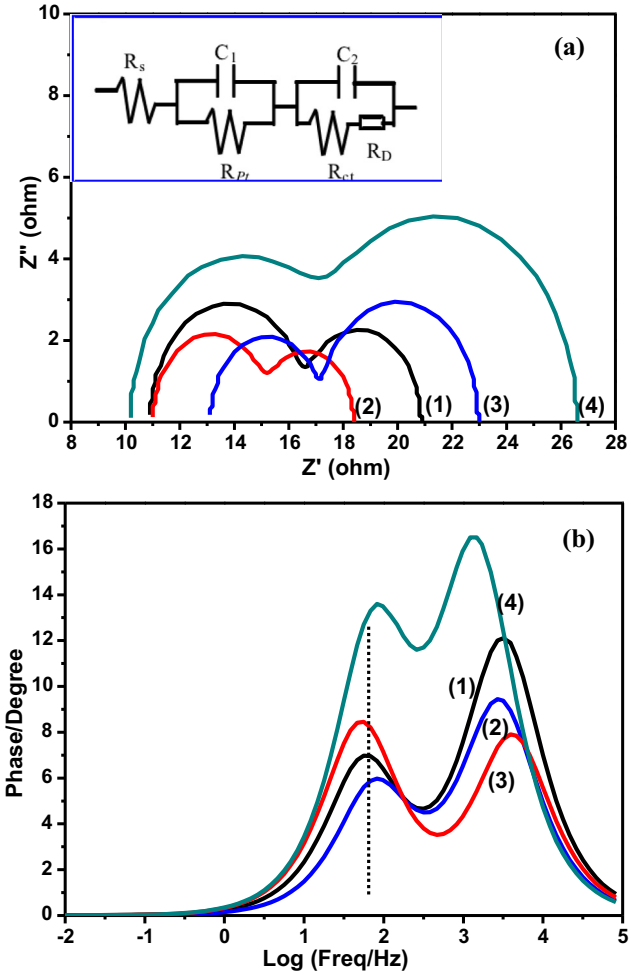

Fig. 6. Results of EIS of (a) Nyquist-plot; (b) Bode-plot curves of the DSSCs modified with different yttrium doping concentrations: (1) TiO_2; (2) TiO_2:0.006 Y; (3) TiO_2:0.015 Y; and (4) TiO_2:0.025 Y. Insert of (a): Employed equivalent circuit model.

Table 2
Summary of EIS measurement results for DSSCs based on different photoanodes.

Samples	R_{Pt} (Ω)	R_{ct} (Ω)	f_{max} (Hz)	Electron lifetime (ms)
Pristine TiO_2	6.5	4.8	58.9	2.77
TiO_2:0.006 Y	4.7	3.7	49.1	3.25
TiO_2:0.006 Y	4.5	6.1	75.9	2.10
TiO_2:0.006 Y	10.6	12.4	81.3	1.96

process between electrolyte and electrons on the conduction band of TiO_2 [38].

EIS analysis

Electrochemical impedance spectroscopy (EIS) was a useful research technique to help understand the charge transfer and recombination dynamics for the prepared DSSCs. In our study, EIS was measured under one sun illumination and V_{oc} bias, and results were shown in Fig. 6. The obtained EIS data was fitted with the ZSimpWin software, and the employed equivalent circuit model was depicted in the insert of Fig. 6a. Typically, the Nyquist plot of DSSC processed two semicircles in the frequency range of this experiment (0.1–10 kHz). The semicircles shown represented the charge transfer resistance at the Pt counter electrode/electrolyte interface (R_{Pt}) in the high frequency region and charge transfer resistance (R_{ct}) associated with charge transfer across the TiO_2 thin film and TiO_2/redox electrolyte interface in the intermediate frequency region, respectively [21]. The EIS parameters of the pristine TiO_2 and yttrium modified TiO_2 based DSSCs were listed in Table 2. It was observed that the cell TiO_2:0.006 Y exhibited a lower R_{ct} than that of cell based on pristine TiO_2, which indicated a more facile electron transfer kinetic across the TiO_2 thin film and TiO_2/redox electrolyte interface and reduced charge recombination level. However, with increased modification concentration, the cell TiO_2:0.015 Y and TiO_2:0.025 Y showed an increased R_{ct}, which may be a result of inhibited charge transfer process [24]. In summary, the R_{ct} firstly decreased and then increased with enhanced doping concentration, which was consistent with the variation trend of J_{sc} and power conversion efficiency of the obtained soar cells. The above variation trends in charge transfer resistance may be ascribed to different existing states of Y_2O_3. On the one hand,formation of yttrium oxide on TiO_2 surface after doping modification may be responsible for decreased R_{ct} value for TiO_2:0.006 Y. The formed Y_2O_3 may be able to passivate the electron traps derivated from surface states of TiO_2 nanocrystal and reduce charge recombination, which is similar to the situation of Al_2O_3 to passivate TiO_2 surface states in Al_2O_3/TiO_2 core-shell structure [39]. On the other hand, similar with previous report on Mg doped TiO_2 thin film [17], we consider TiO_2 nanoparticles thin film may partly collapse and reconstruct during the second annealing process, which would result in some Y_2O_3 remaining among TiO_2 nanoparticles network. As illustrated by research of S. Phadke et al. [40], incorporation of a hierarchical, interconnected network of channels and pores in the TiO_2 film electrode led to a facile electron transfer. However, with increased yttrium doping concentration, excessive Y_2O_3 nanocrystal may randomly immingle among the TiO_2 nanoparticle network, which will compromise the interconnection of TiO_2 network and therefore retard transfer of photogenerated electron among TiO_2 thin film. In addition, as mentioned before, excessive doping led to more traps and defects in the TiO_2 lattice, which could also inhibited electron transfer inside TiO_2 nanocrystal. Based on the reasons discussed above, electron transfer was inhibited under enhanced yttrium doping concentration, and this will result in more chances for charge recombination.

Further information about the electron lifetime could be found in the Bode plots (Fig. 6b), with which the electron life time could be calculated with the following equation [41]:

$$\tau = \frac{1}{2\pi f_{max}}$$

where f_{max} is the frequency position at where the intermediate frequency peak appeared in Bode plot. The f_{max} and calculated electron lifetime of different obtained cells were also included in Table 2. It could be seen the cell TiO_2:0.006 Y owned a prolonged electron lifetime, which is an evidence of reduced electron recombination in the TiO_2 electrode. In summary, it could be deduced from EIS analysis that photogenerated electron lifetime could be prolonged and charge transport resistance could be reduced under moderate yttrium doping, which is favorable for a better photovoltaic performance. However, excessive doping concentration could result in negative influence on the cell's photovoltaic performance.

Conclusion

In summary, a facile hydrothermal method to fabricate yttrium doping TiO_2 nanocrystals was used in our work. Different yttrium doping concentrations were employed to investigate the effects of doping modification on the DSSC's performance. The experimental results showed that compared with pure TiO_2, the enhanced photovoltaic performance may be attributed to its enhanced visible light absorption, improved dye loading capacity, suppressed photogenerated electrons recombination and lower charge transfer resistance. It is hoped that our research could give some information in the further development of DSSCs.

Acknowledgement

This work was mainly supported by the Nation Natural Science Foundation of China (NSFC, Grant No. 51272115; NSFC, Grant No. 61504073 and NSFC, Grant No. 21406123).

References

[1] Li B, Wang L, Kang B, Wang P, Qiu Y. Review of recent progress in solid-state dye-sensitized solar cells. Sol Energy Mater Sol Cells 2006;90:549–73.
[2] Xu F, Zhang X, Wu Y, Wu D, Gao Z, Jiang K. Facile synthesis of TiO_2 hierarchical microspheres assembled by ultrathin nanosheets for dye-sensitized solar cells. J Alloys Compd 2013;574:227–32.
[3] Wee SH, Huang PS, Lee JK, Goyal A. Heteroepitaxial Cu_2O thin film solar cell on metallic substrates. Sci Rep 2015;5:16272.
[4] Minami T, Miyata T, Nishi Y. Relationship between the electrical properties of the n-oxide and p-Cu_2O layers and the photovoltaic properties of Cu_2O-based heterojunction solar cells. Sol Energy Mater Sol Cells 2016;147:85–93.
[5] Williams BA, Mahajan A, Smeaton MA, Holgate CS, Aydil ES, Francis LF. Formation of copper zinc tin sulfide thin films from colloidal nanocrystal dispersions via aerosol-jet printing and compaction. ACS Appl Mater Interfaces 2015;7:11526–35.
[6] Johnson MC, Wrasman C, Zhang X, Manno M, Leighton C, Aydil ES. Self-regulation of Cu/Sn ratio in the synthesis of Cu_2ZnSnS_4 films. Chem Mater 2015;27:2507–14.
[7] O'Regan B, Gratzel M. A low-cost, high-efficiency solar cell based on dye-sensitized colloidal TiO_2 films. Nature 1991;353:737–40.
[8] Caramori S, Cristino V, Boaretto R, Argazzi R, Bignozzi CA, Carlo AD. New components for dye-sensitized solar cells. Int J Photoenergy 2010;2010:58–63.

[9] Chou CS, Yang RY, Yeh CK, Lin YJ. Preparation of TiO_2/Nano-metal composite particles and their applications in dye-sensitized solar cells. Powder Technol 2009;194:95–105.
[10] Kim S, Kim D, Choi H, Kang MS, Song K, Kang SO, et al. Enhanced photovoltaic performance and long-term stability of quasi-solid-state dye-sensitized solar cells via molecular engineering. Chem Commun 2008;40:4951–3.
[11] Lewis NS. Toward cost-effective solar energy use. Science 2007;315:798–801.
[12] Gratzel M. Photoelectrochemical cells. Nature 2001;414:338–44.
[13] Grätzel M. Dye-sensitized solar cells. J Photochem Photobiol C 2003;4:145–53.
[14] Günes SS, Serdar N. Hybrid solar cells. Inorg Chim Acta 2008;361:581–8.
[15] Nazeeruddin MK, Kay A, Rodicio I, Humphry-Baker R, Mueller E, Liska P, et al. Conversion of light to electricity by cis-X_2bis (2,2′-bipyridyl-4,4′-dicarboxylate) ruthenium (II) charge-transfer sensitizers (X = Cl−, Br−, I−, CN−, and SCN−) on nanocrystalline titanium dioxide electrodes. J Am Chem Soc 1993;115:6382–90.
[16] Zalas M, Walkowiak M, Schroeder G. Increase in efficiency of dye-sensitized solar cells by porous TiO_2 layer modification with gadolinium-containing thin layer. J Rare Earths 2011;29:783–6.
[17] Peng T, Fan K, Zhao D, Chen J. Enhanced energy conversion efficiency of Mg^{2+}-modified mesoporous TiO_2 nanoparticles electrodes for dye-sensitized solar cells. J Phys Chem C 2010;114:22346–51.
[18] Nasir M, Bagwasi S, Jiao Y, Chen F, Tian B, Zhang J. Characterization and activity of the Ce and N co-doped TiO_2 prepared through hydrothermal method. Chem Eng J 2014;236:388–97.
[19] Seddon AB, Tang Z, Furniss D, et al. Progress in rare-earth-doped mid-infrared fiber lasers. Opt Express 2010;18:26704–19.
[20] Higuchi T, Hotta Y, Hikita Y, Maruyama S, Hayamizu Y, Akiyama H, et al. LaVO4: Eu Phosphor films with enhanced Eu solubility. Appl Phys Lett 2011;98:071902–3.
[21] Zhang J, Peng W, Chen Z, Chen H, Han L. Effect of cerium doping in the TiO_2 photoanode on the electron transport of dye-sensitized solar cells. J Phys Chem C 2012;116:19182–90.
[22] Liu R, Qiang LS, Yang WD, Liu HY. Enhanced conversion efficiency of dye-sensitized solar cells using Sm_2O_3-modified TiO_2 nanotubes. J Power Sources 2013;223:254–8.
[23] Shogh S, Mohammadpour R, Zad AI, Taghavinia N. Improved photovoltaic performance of nanostructured solar cells by neodymium-doped TiO_2 photoelectrode. Mater Lett 2015;159:273–5.
[24] Wang W, Liu Y, Sun J, Gao L. Nitrogen and yttrium co-doped mesoporous titania photoanodes applied in DSSCs. J Alloys Compd 2016;659:15–22.
[25] Wu J, Xie G, Lin J, Lan Z, Huang M, Huang Y. Enhancing photoelectrical performance of dye-sensitized solar cell by doping with europium-doped yttria rare-earth oxide. J Power Sources 2010;195:6937–40.
[26] Zhao B, Wang J, Li H, Wang H, Jia X, Su P. The influence of yttrium dopant on the properties of anatase nanoparticles and the performance of dye-sensitized solar cells. Phys Chem Chem Phys 2015;17:14836–42.
[27] Xu P, Tang Q, He B, Li Q, Chen H. Transmission booster from SiO_2 incorporated TiO_2 crystallites: enhanced conversion efficiency in dye-sensitized solar cells. Electrochim Acta 2014;134:281–6.
[28] Sleigh C, Pijpers AP, Jaspers A, Coussens B, Meier RJ. On the determination of atomic charge via ESCA including application to organometallics. J Electron Spectrosc Relat Phenom 1996;77:41–57.
[29] Charanpahari A, Umare SS, Gokhale SP, Sudarsan V, Sreedhar B, Sasikala R. Enhanced photocatalytic activity of multi-doped TiO_2 for the degradation of methyl orange. Appl Catal A 2012;443–444:96–102.
[30] Khan M, Li J, Cao W, Ullah A. Advancement in the photocatalytic properties of TiO_2 by vanadium and yttrium codoping: effect of impurity concentration on the photocatalytic activity. Sep Purif Technol 2014;130:15–8.
[31] Niu X, Sujuan LI, Chu H, Zhou J. Preparation, characterization of Y_{3+}-doped TiO_2 nanoparticles and their photocatalytic activities for methyl orange degradation. J Rare Earths 2011;29:225–9.
[32] Zhang W, Wang K, Zhu S, Li Y, Wang F, He H. Yttrium-doped TiO_2 films prepared by means of DC reactive magnetron sputtering. Chem Eng J 2009;155:83–7.
[33] Kumar KS, Song CG, Bak GM, Heo G, Seong MJ, Yoon JW. Phase control of yttrium (Y)-doped TiO_2 nanofibers and intensive visible photoluminescence. J Alloys Compd 2014;617:683–7.
[34] Zhang H, Tan K, Zheng H, Gu Y, Zhang WF. Preparation, characterization and photocatalytic activity of TiO_2 codoped with yttrium and nitrogen. Mater Chem Phys 2011;125:156–60.
[35] Xiong Z, Zhao Y, Zhang J, Zheng C. Efficient photocatalytic reduction of CO_2 into liquid products over cerium doped titania nanoparticles synthesized by a sol–gel auto-ignited method. Fuel Process Technol 2015;135:6–13.
[36] Zhao B, Wang J, Li H, Xu Y, Yu H, Jia X, et al. Solar-to-electric performance enhancement by titanium oxide nanoparticles coated with porous yttrium oxide for dye-sensitized solar cells. ACS Sustainable Chem Eng 2015;3:1518–25.
[37] Lei BX, Zhang P, Qiao HK, Zheng XF, Hu YS, Huang GL, et al. A facile template-free route for synthesis of anatase TiO_2 hollow spheres for dye-sensitized solar cells. Electrochim Acta 2014;143:129–34.
[38] Li ZQ, Que YP, Mo LE, Chen WC, Ding Y, Ma YM, et al. One-pot synthesis of mesoporous TiO_2 micropheres and its application for high-efficiency dye-sensitized solar cells. ACS Appl Mater Interfaces 2015;7:10928–34.
[39] Zhang XT, Liu HW, Taguchi T, Meng QB, Sato O, Fujishima A. Slow interfacial charge recombination in solid-state dye-sensitized solar cell using Al_2O_3-coated nanoporous TiO_2 films. Sol Energy Mater Sol Cells 2004;81:197–203.
[40] Phadke S, Du Pasquier A, Birnie DP. Enhanced electron transport through template-derived pore channels in dye-sensitized solar cells. J Phys Chem C 2011;115:18342–7.
[41] Kern R, Sastrawan R, Ferber J, Stangl R, Luther J. Modeling and interpretation of electrical impedance spectra of dye solar cells operated under open-circuit conditions. Electrochim Acta 2002;47:4213–25.